The Solution Structure of a Tetraheme Cytochrome from *Shewanella frigidimarina* Reveals a Novel Family Structural Motif[†,‡]

Vitor B. Paixão,[§] Carlos A. Salgueiro,[||] Lorraine Brennan,[⊥] Graeme A. Reid,[#] Stephen K. Chapman,[+] and David L. Turner*[,§,@]

Instituto de Tecnologia Química e Biológica, Universidade Nova de Lisboa, Rua da Quinta Grande 6, 2780-156 Oeiras, Portugal, Requimte, CQFB, Requimte, CQFB, Departamento de Química da Faculdade de Ciências e Tecnologia da Universidade Nova de Lisboa, Quinta da Torre, 2829-516 Caparica, Portugal, UCD Conway Institute, UCD School of Agriculture, Food Science and Veterinary Medicine, UCD, Belfield, Dublin 4, Ireland, Institute of Structural and Molecular Biology, University of Edinburgh, Mayfield Road, Edinburgh EH9 3JR, U.K., EaStCHEM, School of Chemistry, University of Edinburgh, West Mains Road, Edinburgh EH9 3JJ, U.K., and School of Chemistry, University of Southampton, Southampton SO17 1BJ, U.K.

Received July 14, 2008; Revised Manuscript Received September 17, 2008

ABSTRACT: The bacteria belonging to the genus *Shewanella* are facultative anaerobes that utilize a variety of terminal electron acceptors which includes soluble and insoluble metal oxides. The tetraheme *c*-type cytochrome isolated during anaerobic growth of *Shewanella frigidimarina* NCIMB400 (*Sfc*) contains 86 residues and is involved in the Fe(III) reduction pathways. Although the functional properties of *Sfc* redox centers are quite well described, no structures are available for this protein. In this work, we report the solution structure of the reduced form of *Sfc*. The overall fold is completely different from those of the tetraheme cytochromes c_3 and instead has similarities with the tetraheme cytochrome recently isolated from *Shewanella oneidensis* (*Soc*). Comparison of the tetraheme cytochromes from *Shewanella* shows a considerable diversity in their primary structure and heme reduction potentials, yet they have highly conserved heme geometry, as is the case for the family of tetraheme cytochromes isolated from *Desulfovibrio* spp.

Bacterial tetraheme *c*-type cytochromes were first discovered in *Desulfovibrio* spp. (*1, 2*). These proteins have approximately 30 amino acids per heme, and each cofactor has bishistidinyl axial coordination and is therefore low-spin in the oxidized and reduced forms.

Several structures of tetraheme cytochromes isolated from *Desulfovibrio* spp. (Dc_3, hereafter) have been determined either by X-ray crystallography or by NMR and show that the heme groups are arranged in very close proximity in a roughly circular fashion (for a review, see ref *3*).

More recently, the bacterial genome sequence of *Geobacter sulfurreducens* and *Shewanella oneidensis* revealed that soluble small multiheme proteins are not exclusive to the *Desulfovibrio* genus (*4*−*7*). Moreover, cytochromes containing three or four heme groups have been identified in bacteria that have the ability to reduce metal oxides (most of them located in the cellular exterior) which suggests an important role for these small proteins in transferring electrons from the cytoplasm to the outer membrane and/or to be used as alternative devices to assist in the energy transduction process (*8, 9*).

Gene disruption experiments have shown that PpcA (a triheme cytochrome containing 71 amino acids from *G. sulfurreducens*) and *Sfc*[1] (a small tetraheme cytochrome with 86 residues from *Shewanella frigidimarina*) are both involved in metabolic pathways leading to the reduction of Fe(III) (*6, 10*).

Structural data reported for PpcA and its homologue cytochrome c_7 isolated from *Desulfuromonas acetoxidans* showed that both proteins share structural homologies with Dc_3 (*11*−*13*). Indeed, the arrangement of the three hemes is closely similar to the heme core of tetraheme cytochromes c_3 isolated from the Desulfovibrionacea family but with heme II deleted together with the region of polypeptide responsible for its binding.

[†] This work was supported by Grants POCI/QUI/58985/2004, POCI/QUI/60060/2004, and PPCDT/QUI/60060/2004 from Fundação para a Ciência e Tecnologia (Portugal). V.B.P. was supported by Grant BD/5830/2001 from Fundação para a Ciência e Tecnologia (Portugal).

[‡] The structure data and the chemical shifts are deposited in the Protein Data Bank as entry 2k3v and in the BioMagResBank as entry 15765, respectively.

* To whom correspondence should be addressed: Instituto de Tecnologia Química e Biológica, Universidade Nova de Lisboa, Rua da Quinta Grande 6, 2780-156 Oeiras, Portugal. Telephone: 351 21 4469821. Fax: 351 21 4428766. E-mail: turner@itqb.unl.pt.

[§] Instituto de Tecnologia Química e Biológica, Universidade Nova de Lisboa.

[||] Departamento de Química da Faculdade de Ciências e Tecnologia da Universidade Nova de Lisboa.

[⊥] UCD.

[#] Institute of Structural and Molecular Biology, University of Edinburgh.

[+] School of Chemistry, University of Edinburgh.

[@] University of Southampton.

[1] Abbreviations: *Sfc*, *S. frigidimarina* NCIMB400 tetraheme cytochrome; *Soc*, *S. oneidensis* MR-1 tetraheme cytochrome; $Sffcc_3$, *S. frigidimarina* NCIMB400 flavocytochrome c_3; rmsd, root-mean-square deviation.

10.1021/bi801326j CCC: $40.75
Published on Web 10/25/2008

The periplasmic tetraheme cytochrome produced by the bacteria *S. frigidimarina* (*Sfc*) is even smaller than Dc_3. It contains only approximately 20 amino acid residues per heme group and is the smallest tetraheme cytochrome described to date. Sequence analysis of this cytochrome showed that the heme binding motifs are different from those of Dc_3 (*14*).

Little structural information is available for *Sfc*, and only a preliminary model determined with a limited number of distance constraints was used to predict the heme arrangement in solution (*14*). However, it was possible to show that in *Sfc* the heme groups have a linear arrangement instead of the circular one found in Dc_3. A similar disposition of hemes has been found only in the N-terminal cytochrome domain of a flavocytochrome c_3 ($Sffcc_3$) isolated from the same bacterium (*15, 16*) and in a small tetraheme cytochrome isolated from *S. oneidensis* (*Soc*) (*17*).

Harada and co-workers (*18*) determined the heme redox potentials for *Soc* and the order in which the hemes become oxidized. The thermodynamic properties of the *Sfc* redox centers were also determined (*19*), showing that the cofactors are not structurally or functionally equivalent, with negative and different reduction potentials. As with Dc_3, the reduction potentials of the hemes in *Sfc* are modulated by redox interactions between the four hemes and by redox-Bohr interactions between the hemes and a protonatable center.

Most importantly, the thermodynamic properties of *Soc* and *Sfc* are quite different. Significant differences were also observed for Dc_3 isolated from different species. In fact, from eight different Dc_3 forms, only two very closely related ones exhibited the same order of oxidation of the heme groups (*3, 20*). The wide variations in the sequences and properties of these multiheme proteins make the high degree of conservation of the heme geometry still more surprising.

To rationalize the thermodynamic parameters of *Sfc* and to establish how closely the heme geometry is conserved between *Sfc* and *Soc*, it is necessary to obtain more detailed structural information. Attempts to crystallize *Sfc* were unsuccessful, and in this study, we report the solution structure of the reduced form of *Sfc* and the structural basis for the network of cooperativities observed in this protein are discussed.

MATERIALS AND METHODS

Bacterial Growth and Protein Purification. *S. frigidimarina* cells were grown, and the tetraheme cytochrome was purified as previously described (*6*).

NMR Sample Preparation. For NMR experiments in H_2O, the protein was lyophilized from H_2O and suspended in a 92% H_2O/8% ^2H_2O mixture to a final concentration of approximately 3 mM. For NMR experiments in ^2H_2O, the protein was lyophilized several times from ^2H_2O and then dissolved in ^2H_2O (99.96%) to a final concentration of approximately 3 mM. The pH was adjusted to 6.1 in an anaerobic chamber (Mbraun MB 150 I) by addition of 0.1 M NaO^2H or ^2HCl for ^2H_2O samples and 0.1 M NaOH or HCl for H_2O samples. The pH values measured are direct meter readings without correction for isotope effects (*21*). Complete reduction of the samples was achieved by the reaction with hydrogen gas in the presence of catalytic amounts of hydrogenase isolated from *Desulfovibrio gigas* and *Desulfovibrio vulgaris*. An antibiotic cocktail (70 μM ampicillin, 50 μM kanamycin, and 50 μM chloramphenicol) was added to the sample in H_2O to prevent bacterial growth.

NMR Spectroscopy. All ^1H NMR spectra were obtained on a Bruker DRX-500 spectrometer equipped with a 5 mm inverse detection probe head with an internal B_0 gradient coil and a Eurotherm 818 temperature control unit. All two-dimensional (2D) NMR spectra were acquired at 303 K. Acquisition was made in the phase sensitive mode by the States−TPPI method (*22*) collecting 4096 (t_2) × 1024 (t_1) data points to cover a sweep width of 8 kHz, with 32 scans per increment. NOESY spectra (*23, 24*) were recorded with mixing times of 40, 60, 80, and 100 ms. NOESY spectra of the ^2H_2O samples were recorded with standard pulse sequences with continuous low-power water presaturation during the relaxation delay and the mixing time. NOESY spectra of the H_2O sample were recorded with presaturation of the water resonance by a composite 180° inversion pulse followed by a SCUBA sequence to facilitate recovery of potentially saturated α protons (*25*). Total correlation spectra were acquired using the clean TOCSY pulse sequence (*26*−*28*) with spin-lock times of 40 and 60 ms. DQF-COSY spectra were also acquired (*29, 30*). Data were processed using XWIN-NMR (Bruker, Rheinstetten, Germany). Proton chemical shifts were calibrated using the water signal as an internal reference.

Assignment and Integration. XEASY (version 1.2; ETH, Zurich, Switzerland) (*31*) was used to display and annotate spectra. Amino acid residue assignment was performed using the classical approach described by Wüthrich (*32*). Examination of TOCSY and COSY spectra in H_2O and ^2H_2O allowed spin system identification. Further analysis of the NOESY spectra and identification of H^N-H^N, H^N-H^α, and H^N-H^β connectivities between different spin systems allowed the sequential assignment. Stereospecific assignments were obtained in the process of structure calculation with the aid of GLOMSA (*33*). The assigned NOESY cross-peaks were integrated and converted into volume restraints with SPARKY (*34*). All NOEs were measured in the 80 ms NOESY spectra at 303 K and pH 6.1. Cross-peaks due to protons separated by fixed distances and all intraheme cross-peaks, except those involving the propionate groups, were excluded. Integration was performed by Gaussian and Lorentzian function fitting for isolated peaks and with sum data heights in a box or ellipse surrounding the peak for more overlapped peaks. The baseline around each individual peak was determined and used to correct the measured volume.

Determination of Restraints. Signals from H^α protons close to the H_2O frequency, whenever possible, were taken from the ^2H_2O spectra only, except for H^N-H^α cross-peaks. NOE cross-peaks involving nonexchangeable protons were integrated both in H_2O and in ^2H_2O spectra. These calculated volumes were also used to obtain an overall scaling factor relating the spectra (*35*); the volumes were then combined into a single data set. The smallest recognizable peaks in the H_2O spectra were used to assess the minimum uncertainty volume (δV) for input in INDYANA (*36*) for structure calculation. The program generates upper limit volumes (upv) as $\langle V\rangle + \max(\Delta V,\delta V)$ and lower limit volumes (lov) as $\langle V\rangle - \delta V$, where $\langle V\rangle$ and ΔV are the average and difference of volumes for each pair of symmetrical cross-peaks, respectively. For overlapping peaks involving protons not separated by a fixed distance, upper volume limits (lower distance

constraints) were applied to each possible proton pair. When the structure was calculated, some of the potentially overlapping peaks were specifically assigned as the various possibilities were eliminated by reference to the structure. Hence, a lower limit could also be applied. For the degenerate H^{δ} and H^{ε} ring protons of fast-flipping residues, it is often possible to identify which side of the ring is involved because of the large distance between them. In the preliminary stages of structure calculation, all cross-peaks from degenerate ring protons are treated as nonspecific, with the exception of one chosen to distinguish the two sides of the ring. During structure refinement, individual NOEs were assigned specifically as in the case of nondegenerate protons, with the aid of GLOMSA.

Additional Restraints. Three nonstandard residues were used for structure calculations: fast-flipping aromatic residues with pseudoatoms to limit the orientations of the planes (*35, 37, 38*), flexible heme groups, and proline residues with fixed upper limit distances for ring closure (*35, 36, 39*). In the final stages of structure refinement, the calculated structures were checked for short (<2.5 Å) distances between assigned protons that should give rise to significant NOEs. Even if no peaks were visible at the predicted frequencies, the volume was measured and used in further calculations. In this way, a lower limit distance restraint defines a minimum distance between protons if there is no NOE in the spectra.

Structure Calculation and Analysis. Structure calculations were performed using the extended version of DYANA (*40*), called PARADYANA. This version of DYANA is modified to accept peak volumes as input and pseudocontact shifts for paramagnetic proteins. The functionality of the original DYANA program remains, as well as the extensions introduced in INDYANA (*36*) for the fully automatic conversion of peak volumes into distance constraints. CHIMERA (version 1.24) (*41*) was used for visual interpretation with the preliminary structure calculations, as an aid to assignment, during structure refinement. MOLMOL (version 2.0) (*42*) was used for superimposition, visual inspection, and calculation of mean structure and of root-mean-square deviations from the mean structure. It was also used for calculation of solvent accessible surfaces using a radius of 1.4 Å for the H_2O molecule. Stereochemical analysis of the structures was performed with WHAT IF (version 20030529-0952) (*43*). Identification and classification of the consensus secondary structure elements in the NMR structure ensemble, defined as those present in at least 50% of the structures, were accomplished with PROMOTIF (version 2.0) (*44*).

Secondary structural shifts, which are dominated by the effect of heme ring currents, were calculated for the structures using TOTAL (*45*).

RESULTS

Sequential Assignment. Sequence-specific assignment was straightforward, but no connectivities involving residue 1 were assigned, probably because of the high flexibility of the N-terminus. Sequential connectivities among H^N, H^{α}, and H^{β} protons are shown in Figure S1 of the Supporting Information. All of the residues, with exception of prolines (residues 24, 51, 64, and 73), show at least one of the sequential connectivities between its H^N proton and the H^N, H^{α}, or H^{β} proton of the preceding residue. For the proline residues, connectivities were obtained at least between the H^{δ} protons of the prolines and the H^{α} or H^{β} proton of the preceding residue.

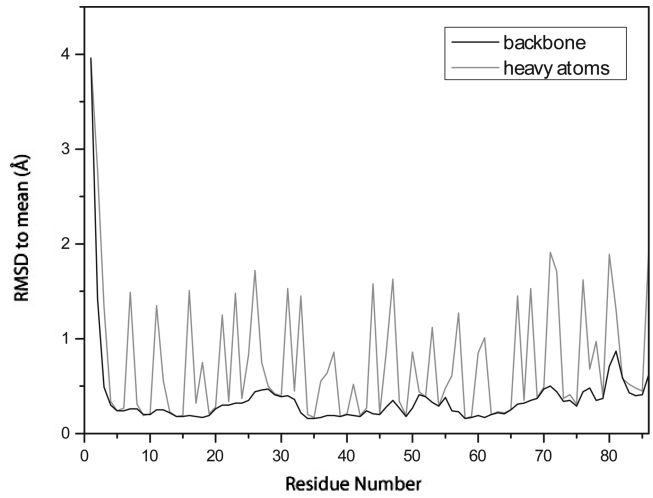

FIGURE 1: Average backbone and heavy atom rmsd values per residue with respect to the mean structure of the family of 20 conformers obtained for *Sfc*.

In total, 86% of all protons in the protein were assigned. This corresponds to 92% of the protons after exclusion of exchangeable protons other than the backbone H^N proton. The chemical shifts have been deposited in the BioMagResBank as entry 15765.

Restraints and Structure Calculations. Assigned cross-peaks in the H_2O and ^2H_2O NOESY spectra were integrated and converted into volume restraints, resulting in 1153 lower limits for volumes (lovs) and 1366 upper limits (upvs). These were used as input for PARADYANA together with a set of 88 fixed upper limit distances (associated with ring closure in the flexible proline residues and heme groups, and the attachment of His ligands) (*35, 36, 39*).

The preliminary structures were also analyzed using GLOMSA (*33*) modified to take NOE volumes as input, and 29 stereospecific assignments were made for diastereotopic pairs of protons or methyl groups. The effect of spin diffusion introduces an uncertainty into the conversion of experimental data to distance constraints. These effects were simulated by complete relaxation matrix calculations based on the initial protein structures, and accordingly, a parameter was set in PARADYANA to loosen all distance restraints by 5%. An average of 29 NOE restraints per amino acid residue (13 lovs and 16 upvs) and 126 per heme residue (58 lovs and 68 upvs) was used for the final calculation (Figure S2 of the Supporting Information).

Quality Analysis of the Structures. The final family consists of 20 structures with the target function increasing by 11% from the first to the last. The structures superimpose with an average backbone rmsd of 0.60 Å and a heavy atom rmsd of 0.95 Å with respect to the mean structure; the values for each residue are shown in Figure 1.

The Ramachandran plot shows 59% of the residues in the most favored regions, 35% in the additionally allowed regions, and 6% in the generously allowed regions. A total of 90 hydrogen bonds were identified in the family of 20 structures with WHAT IF (using routine HBO), 35 of which

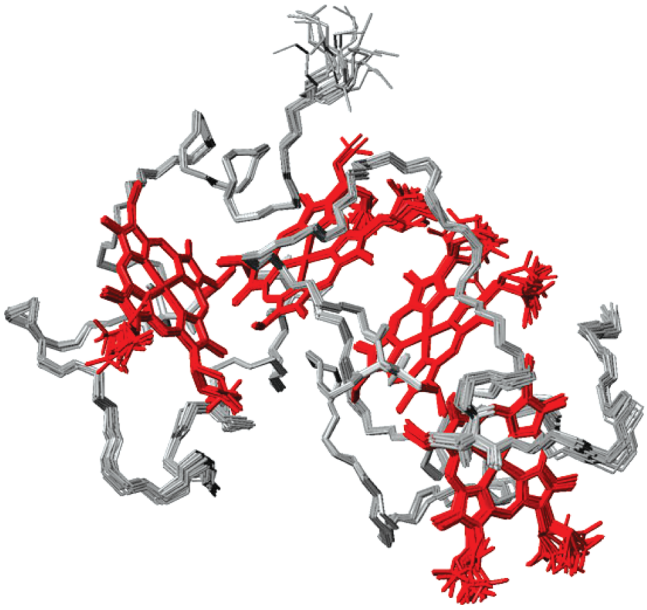

FIGURE 2: Overlay of the 20 lowest-energy NMR structures of *S. frigidimarina* tetraheme cytochrome at pH 6.1. Superimposition was performed using all the heavy atoms. The peptide chain and the hemes are color-coded gray and red, respectively. In this orientation, the N-terminus is at the top left and hemes are disposed from left to right in the following order: I, II, III, and IV. This figure was produced using MOLMOL (*42*).

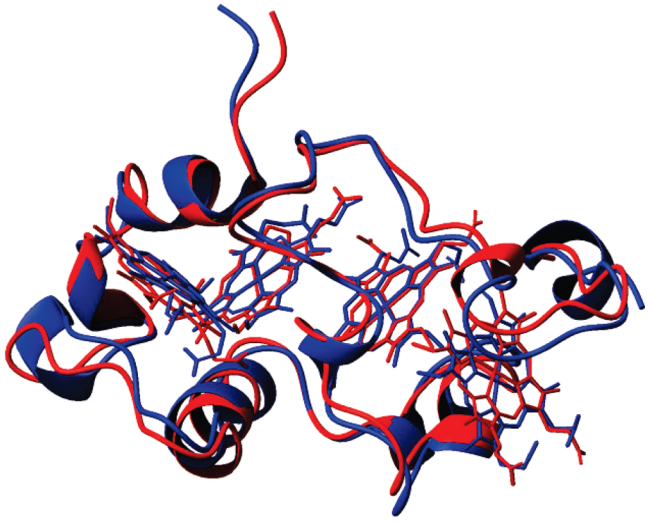

FIGURE 3: Comparison of the *Sfc* (red) and *Soc* (blue) structures. The lowest-energy NMR structure of *Sfc* is superimposed on the X-ray structure of *Soc*. This figure was generated using MOLMOL (*42*).

were present in at least 50% of the structures. The NMR structure models presented in Figure 2 are, in general, well-defined. Some amino acid side chains or heme ligand propionate groups show a larger conformational variability probably because of the reduction in the number of restraints due to higher level of solvent exposure.

DISCUSSION

Comparison of the Sfc and Soc Structures. Sfc is folded in a series of helices connected by extended loop regions; there are no β-strands (Figure 3). Three α-helices are established between residues Ala^{5} and Val^{10} (A), Ala^{29} and Gln^{34} (B), and Cys^{58} and Cys^{61} (C), and there are three additional 3_{10}-helical regions between residues Cys^{15} and Asn^{17}, Leu^{42} and Glu^{44}, and Cys^{75} and Thr^{77}. The four bis-histidinyl heme groups are arranged in a linear fashion with hemes I and II and hemes III and IV exhibiting a perpendicular orientation of heme planes, whereas the planes of the central hemes, II and III, are roughly parallel to each other.

When the available sequences for *Sfc* and *Soc* are compared, 27 residues are different, plus the five extra residues at the C-terminus of *Soc* (Figure 4). Comparison of the reduced NMR structures of *Sfc* with the X-ray structure of *Soc* (*17*) reveals that the general folds of the proteins, as well as the relative position of the four heme groups, are similar (Figure 3 and Table 1). However, differences are observed in the helical regions. The α-helices in *Soc* are established between residues Leu^{5} and Ala^{10} (A), Ala^{29} and His^{39} (B), and Ser^{85} and Leu^{89} (C), and there are 3_{10}-helical regions between residues Leu^{42} and Glu^{44}, Lys^{50} and His^{52}, and Cys^{58} and Asp^{60} (Figure 4). The first two α-helices are formed in the same region of the two proteins. However, α-helix B in *Soc* is five residues longer, and *Soc* α-helix C is formed at the C-terminal end of the protein and involves three of the five extra residues which are not present in *Sfc*. In *Sfc*, α-helix C is established between the two Cys residues that form the heme III binding motif. Both proteins have three 3_{10}-helical regions, but only that involving residues Leu^{42}−Glu^{44} is conserved.

The heme spatial disposition in *Sfc* and *Soc* is highly conserved with average iron−iron distances differing by less than 6% between the structures (Table 1). However, important differences were detected in the orientation of the rings of the axial heme ligands and the dihedral angles formed between them. Indeed, with the exception of heme II, where the angles are similar, at least one His axial ligand of each heme has a different orientation in *Sfc* and *Soc*. This is the case for His67 (heme I), His64 (heme III), and both His^{52} and His^{79} in heme IV. These differences are likely to affect the redox properties of the heme groups and the rates of heme−heme electron transfer (see below).

Comparison of Sfc and the N-Terminal Domain of Flavocytochrome c_3 Structures. Sequence comparison of *Sfc* and the N-terminal domain of flavocytochrome c_3, an enzyme with fumarate reductase activity (42% identical), also isolated from *S. frigidimarina* (*Sffcc$_3$*) showed that the heme binding motifs (CXXCH) and the sixth heme axial ligands are strictly conserved (Figure 4). The X-ray structure of *Sffcc$_3$* was determined (*15*), and comparison with the *Sfc* structure shows remarkably similar distances among hemes I, II, and III, with differences of <2%. However, whereas the polypeptide chain traces of *Sfc* and *Sffcc$_3$* are similar from the N-terminus up to Ala^{67}, the C-terminal region of *Sfc* is unlike that of *Sffcc$_3$* because of the interaction with the FAD binding domain, which results in a nearly 60° angle difference between the heme IV planes of the two proteins, and differences of up to 29% are observed for distances to heme IV.

In view of the differences in thermodynamic properties of *Sfc* and *Soc* that exist despite the close similarity in their structures, it would be unwise to use these properties to model the behavior of the N-terminal domain of *Sffcc$_3$* with its much larger structural differences. Indeed, the order of oxidization of the hemes in *Sffcc$_3$* has been determined (*46*) and shows no correlation with that of *Sfc* (*14*).

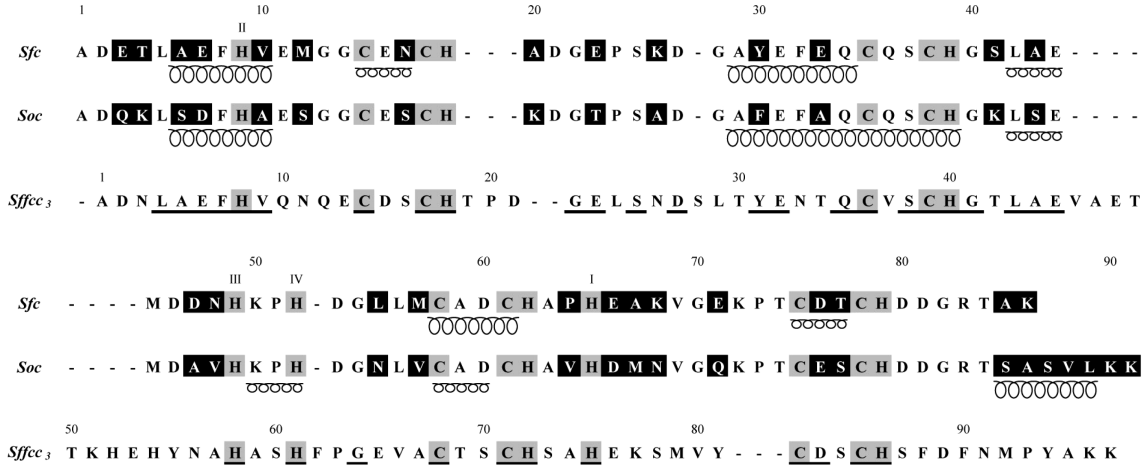

FIGURE 4: Sequence alignment of tetraheme cytochromes from *S. frigidimarina* (*Sfc*) and *S. oneidensis* (*Soc*) and *S. frigidimarina* flavocytochrome c_3 (*Sffcc*$_3$). Large and small coils denote α-helices and 3_{10}-helices, respectively. The nonconserved residues between the *Sfc* and *Soc* proteins are highlighted in black. The cysteines and histidines that bind to the hemes are highlighted in gray, and Roman numbers (I−IV) refer to the sixth heme axial ligand. The conserved residues between *Sfc* and *Sffcc*$_3$ are underlined in the latter sequence.

Table 1: Average Iron−Iron Distances (angstroms) in the NMR (*Sfc*) and X-ray (*Soc*) Reduced Structures[a]

		heme I	heme II	heme III
heme II	*Sfc*	12.8 (0.03)		
	Soc	12.0		
	Sffcc$_3$	12.5		
heme III	*Sfc*	17.2 (0.07)	9.6 (0.1)	
	Soc	16.3	9.2	
	Sffcc$_3$	17.3	9.5	
heme IV	*Sfc*	23.2 (0.11)	20.0 (0.08)	11.0 (0.03)
	Soc	23.1	19.9	11.2
	Sffcc$_3$	29.8	25	15.6

[a] Values in parentheses correspond to the standard deviation for the family of 20 NMR conformers. The iron−iron distances of the highly homologous N-terminal domain of flavocytochrome c_3 (*Sffcc*$_3$) are also given for comparison.

Structural Basis for the Electrostatic Origin of the Sfc Redox Interactions. The thermodynamic properties of the hemes in *Sfc*, including the reduction potentials and heme−redox (heme−heme) interactions, have been determined (*19*). The values obtained for the heme−redox interactions suggest that they are dominated by electrostatic effects, rather than conformational changes between redox stages. Indeed, the redox interactions between the heme groups are all positive such that the oxidation of a particular heme makes the oxidation of its neighbors more difficult (negative homocooperativity). On the other hand, the redox interactions with the redox-Bohr center are all negative; i.e., the oxidation of the hemes facilitates deprotonation of the redox center and vice versa (positive heterocooperativity). The correlation obtained for the distance and the redox interactions between pairs of hemes (Figure 5) further supports the electrostatic origin of the redox interactions. The correlation between the redox interaction values obtained for *Soc* by Harada and co-workers (*18*) and the Fe−Fe distances taken from the *Soc* X-ray structure (*17*) is not so clearly electrostatic in origin (Figure 5). However, it should be noted that in *Soc* analysis the redox-Bohr interactions were not separated from heme−heme interactions.

Structural Mapping of the Heme Reduction Potentials. As described above, heme−redox interactions modulate the reduction potentials of the heme groups during the oxidation of the protein such that the order of oxidation is not necessarily the same as the order of potentials in the fully reduced protein. The order in which the hemes are oxidized is different in *Sfc* and *Soc*: it is IV−II−I−III for *Sfc* (*19*) and I−II−(III,IV) for *Soc* (*18*). Of the 27 residues where the two proteins differ, 11 residues involve charge alteration: residues 3, 23, 26, 33, 47, 68, 71, and 86 are potentially charged in *Sfc* and are not charged in *Soc*, whereas residues 4, 20, and 41 become charged in *Soc*. Additionally, *Soc* has also two extra positive residues at the C-terminus (Figure 4). Overall, compared with *Soc*, *Sfc* has four extra negatively charged residues and three fewer positively charged. The substitutions are not localized in any particular region of the protein, and most of them occur at protein surface; however, the protein is small, and the more negatively charged protein surface in *Sfc* might contribute to the differences observed in the heme reduction potentials.

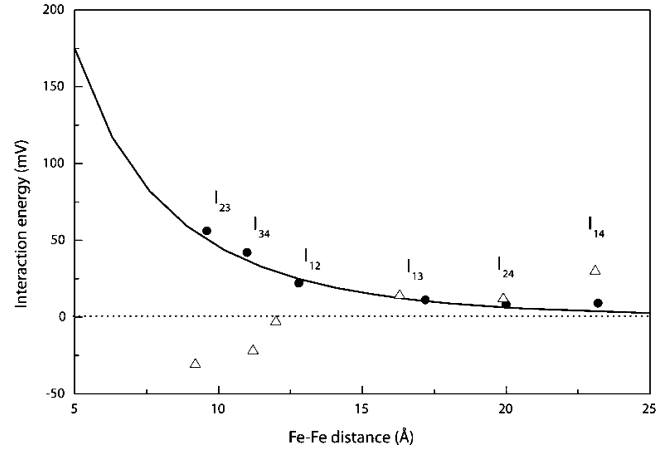

FIGURE 5: Distance dependence of the pairwise interaction energies between the iron centers (I_{ij}, interaction between hemes *i* and *j*; *i* and *j* = 1−4; *i* > *j*). The black circles indicate the correlations obtained for *Sfc*. Triangles correlate the pairwise interaction values obtained by Harada and co-workers (*18*) for *Soc* and distances taken from the *Soc* crystal structure (*16*). The solid line was obtained with an exponentially decaying Coulomb interaction considering an effective dielectric constant of 8.6 (0.6) and Debye length of 7.7 (0.3) Å, as previously reported (*19*).

The midpoint reduction potentials of *Sfc* at pH 7 are −215, −190, −175, and −125 mV for hemes IV, II, I, and III,

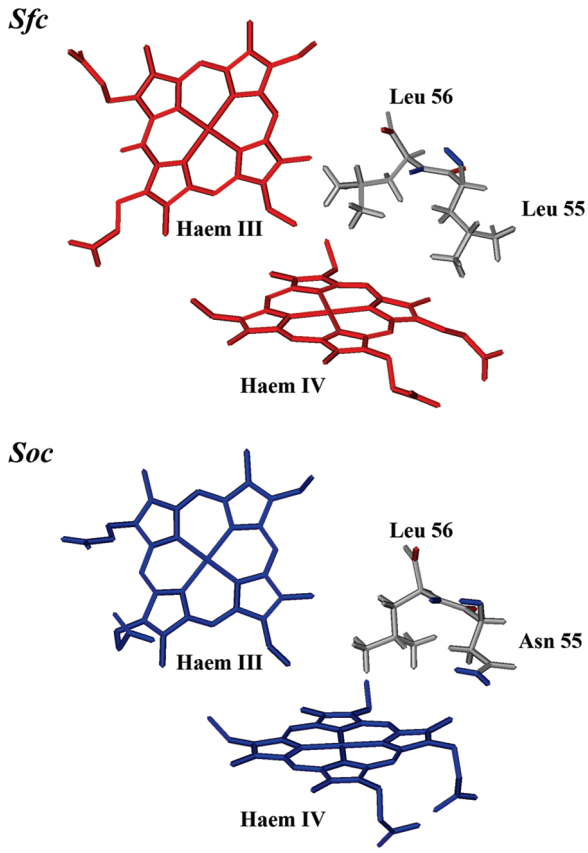

FIGURE 6: Relative position of hemes III and IV and residues 55 and 56 for *Sfc* (best NMR structure) and *Soc* [X-ray structure (*16*)]. Hemes III and IV have the same orientations in both structures.

respectively (*19*). The reduction potential of heme III is clearly the least negative, so it dominates the last oxidation step of *Sfc*. Assuming that there is little change in conformation between the reduced and oxidized forms, this correlates well with the fact that heme III is by far the least solvent-exposed (345, 305, 196, and 385 Å^2 for hemes I, II, III, and IV, respectively). Heme III also has the lowest level of solvent exposure in *Soc*, but its reduction potential in the last step of oxidation is more negative (−186 mV) than in *Sfc* and similar to that of heme IV (*18*).

The higher reduction potential of heme III in *Sfc* in comparison with that of *Soc* may be influenced by the replacement of residue Asn^{55} in *Soc* with the hydrophobic residue (Leu^{55}) in *Sfc*. This residue forces the side chain of the conserved residue Leu^{56} to orient toward heme III, creating a more hydrophobic environment (Figure 6).

Another important change between the two proteins is observed in the side chain orientation of conserved residue Lys^{72}. This residue in the reduced *Soc* protein is hydrogen bonded to propionate group P17 of heme II (P_{17}^{II}), whereas the side chain of Lys^{72} in *Sfc* is reoriented toward propionate P13 of heme III (P_{13}^{III}) (Figure 7). Placing a positive charge close to heme III of *Sfc* helps to stabilize the reduced form of this heme and thus contributes to the high reduction potential of heme III in *Sfc*.

The solvent exposure of the remaining heme groups is similar and much greater than that of heme III. Since the reduction potentials of hemes I, II, and IV differ by less than 40 mV in both *Sfc* and *Soc*, a variety of subtle effects could easily be as important as the solvent effect. One possible effect is the geometry of the dihedral angle of the His rings and the heme porphyrin planes. Indeed, studies carried out in several cytochromes showed that changes in the angle formed between the His ring planes and those of the heme porphyrin may account for changes of up to 30 mV in the heme redox potentials (*39, 47*−*49*).

Structural Mapping of the Redox-Bohr Center. Previous studies showed the individual reduction potentials of the heme groups (microscopic potentials) in *Sfc* are pH-dependent, with heme III being by far the most affected. The redox-Bohr interaction, i.e., the measure of the effect of the redox-Bohr center deprotonation on the reduction potential of the hemes, is −36 mV for heme III but −9, −11, and −4 mV for hemes I, II, and IV, respectively (*19*), and the sign of the interactions is that expected for an electrostatic effect between an electron and a proton.

Thus, the ionizable center responsible for the redox-Bohr effect in *Sfc* is close to heme III and may well be a propionate group of that heme. In the case of *Soc*, it was suggested that the redox-Bohr center should be located close to heme II since Lys^{72} is hydrogen bonded to propionate group P_{17}^{II} in the reduced form (Figure 7). It is interesting to note that the conserved residue Lys^{72} adopts a completely different orientation in *Sfc*. Indeed, in the reduced structure of *Sfc*, the N^Z protons of Lys^{72} are oriented toward heme III and therefore are pointing away from P_{17}^{II} (Figure 7).

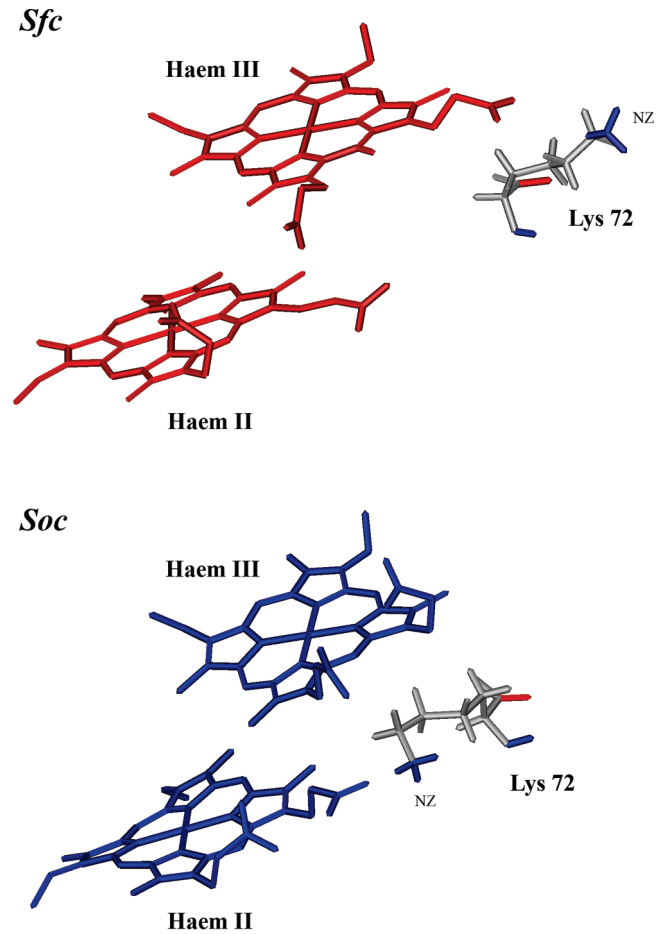

FIGURE 7: Relative position of hemes II and III and the conserved positively charged residue Lys^{72} for *Sfc* (best NMR structure) and *Soc* [X-ray structure (*16*)]. Hemes III and IV have the same orientations in both structures.

CONCLUSIONS

The structure of the reduced tetraheme cytochrome from *S. frigidimarina* is the first solution structure of a multiheme cytochrome isolated from *Shewanella* spp. The protein folds in a series of helices with no β-strands present. The heme groups are arranged in a linear fashion with hemes I and II and hemes III and IV exhibiting a perpendicular orientation of heme planes, whereas the planes of central hemes II and III are nearly parallel to each other. The structure shows close similarities with the X-ray structure determined for the tetraheme cytochrome from *S. oneidensis* (*17*), with rearrangements of the side chains of two conserved residues (Leu^{56} and Lys^{72}) that influence the properties of the redox centers in the two proteins.

Comparison of the structures suggests that the small tetraheme cytochromes isolated from *Shewanella* spp. represent a new structural motif that is distinct from that of the tetraheme cytochromes c_3 from the Desulfovibrionacea family (Dc_3). A similar motif, with some rearrangement of heme IV, is found in the N-terminal cytochrome domain of a flavocytochrome c_3 ($Sffcc_3$) isolated from *S. frigidimarina* (*15, 16*). The most remarkable feature of these motifs is that the architecture of the heme core is highly conserved despite a low degree of sequence homology. The purpose of this conserved geometry is certainly not obvious because the thermodynamic properties of the hemes, including homo- and heterocooperativities as well as the reduction potentials, differ substantially among Dc_3 and are also variable within the *Shewanella* spp. structural motif.

In the case of Dc_3, which are thought to transport pairs of electrons between the periplasmic hydrogenases and transmembrane electron transfer complexes, the geometry is likely to be important for the efficient transfer of consecutive electrons. Although Dc_3 may be adapted to the specific conditions of different organisms, their properties within the electron transfer complexes are also likely to depend on those of their partners. Understanding the diverse properties within the new family of *Shewanella* tetraheme cytochromes will probably also require a detailed study of their electron transfer partners.

SUPPORTING INFORMATION AVAILABLE

Two tables of restraints used for the structure calculation, one figure with sequential NOE connectivities, and one figure with the number of constraints per residue. This material is available free of charge via the Internet at http://pubs.acs.org.

REFERENCES

1. Postgate, J. R. (1954) Presence of cytochrome in a obligate anaerobe. *Biochem. J. 56*, xi–xii.
2. Ishimoto, M. K., Koyama, J., and Nagai, Y. (1954) A cytochrome and a green pigment of sulphate-reducing bacteria. *Bull. Chem. Soc. Jpn. 27*, 564–564.
3. Louro, R. O. (2007) Proton thrusters: Overview of the structural and functional features of soluble tetrahaem cytochromes c3. *J. Biol. Inorg. Chem. 12*, 1–10.
4. Seeliger, S., Cord-Ruwisch, R., and Schink, B. (1998) A periplasmic and extracellular c-type cytochrome of *Geobacter sulfurreducens* acts as a ferric iron reductase and as an electron carrier to other acceptors or to partner bacteria. *J. Bacteriol. 180*, 3686–3691.
5. Afkar, E., and Fukumori, Y. (1999) Purification and characterization of triheme cytochrome c7 from the metal-reducing bacterium, *Geobacter metallireducens*. *FEMS Microbiol. Lett. 175*, 205–210.
6. Gordon, E. H., Pike, A. D., Hill, A. E., Cuthbertson, P. M., Chapman, S. K., and Reid, G. A. (2000) Identification and characterization of a novel cytochrome c_3 from *Shewanella frigidimarina* that is involved in Fe(III) respiration. *Biochem. J. 349*, 153–158.
7. Tsapin, A. I., Nealson, K. H., Meyers, T., Cusanovich, M. A., Van Beuumen, J., Crosby, L. D., Feinberg, B. A., and Zhang, C. (1996) Purification and properties of a low-redox-potential tetraheme cytochrome c_3 from *Shewanella putrefaciens*. *J. Bacteriol. 178*, 6386–6388.
8. Mahadevan, R., Bond, D. R., Butler, J. E., Esteve-Nunez, A., Coppi, M. V., Palsson, B. O., Schilling, C. H., and Lovley, D. R. (2006) Characterization of metabolism in the Fe(III)-reducing organism *Geobacter sulfurreducens* by constraint-based modeling. *Appl. Environ. Microbiol. 72*, 1558–1568.
9. Pessanha, M., Morgado, L., Louro, R. O., Londer, Y. Y., Pokkuluri, P. R., Schiffer, M., and Salgueiro, C. A. (2006) Thermodynamic characterization of triheme cytochrome PpcA from *Geobacter sulfurreducens*: Evidence for a role played in e^-/H^+ energy transduction. *Biochemistry 45*, 13910–13917.
10. Lloyd, J. R., Leang, C., Hodges Myerson, A. L., Coppi, M. V., Cuifo, S., Methe, B., Sandler, S. J., and Lovley, D. R. (2003) Biochemical and genetic characterization of PpcA, a periplasmic c-type cytochrome in *Geobacter sulfurreducens*. *Biochem. J. 369*, 153–161.
11. Pokkuluri, P. R., Londer, Y. Y., Duke, N. E., Long, W. C., and Schiffer, M. (2004) Family of cytochrome c7-type proteins from *Geobacter sulfurreducens*: Structure of one cytochrome c7 at 1.45 Å resolution. *Biochemistry 43*, 849–859.
12. Czjzek, M., Arnoux, P., Haser, R., and Shepard, W. (2001) Structure of cytochrome c7 from *Desulfuromonas acetoxidans* at 1.9 Å resolution. *Acta Crystallogr. D57*, 670–678.
13. Coutinho, I. B., Turner, D. L., Liu, M. Y., LeGall, J., and Xavier, A. V. (1996) Structure of the three-haem core of cytochrome c551.5 determined by ^{1}H NMR. *J. Biol. Inorg. Chem. 1*, 305–311.
14. Pessanha, M., Brennan, L., Xavier, A. V., Cuthbertson, P. M., Reid, G. A., Chapman, S. K., Turner, D. L., and Salgueiro, C. A. (2001) NMR structure of the haem core of a novel tetrahaem cytochrome isolated from *Shewanella frigidimarina*: Identification of the haem-specific axial ligands and order of oxidation. *FEBS Lett. 489*, 8–13.
15. Taylor, P., Pealing, S. L., Reid, G. A., Chapman, S. K., and Walkinshaw, M. D. (1999) Structural and mechanistic mapping of a unique fumarate reductase. *Nat. Struct. Biol. 6*, 1108–1112.
16. Leys, D., Tsapin, A. S., Nealson, K. H., Meyer, T. E., Cusanovich, M. A., and Van Beeumen, J. J. (1999) Structure and mechanism of the flavocytochrome c fumarate reductase of *Shewanella putrefaciens* MR-1. *Nat. Struct. Biol. 6*, 1113–1117.
17. Leys, D., Meyer, T. E., Tsapin, A. S., Nealson, K. H., Cusanovich, M. A., and Van Beeumen, J. J. (2002) Crystal structures at atomic resolution reveal the novel concept of "electron-harvesting" as a role for the small tetraheme cytochrome c. *J. Biol. Chem. 277*, 35703–35711.
18. Harada, E., Kumagai, J., Ozawa, K., Imabayashi, S., Tsapin, A. S., Nealson, K. H., Meyer, T. E., Cusanovich, M. A., and Akutsu, H. (2002) A directional electron transfer regulator based on heme-chain architecture in the small tetraheme cytochrome c from *Shewanella oneidensis*. *FEBS Lett. 532*, 333–337.
19. Pessanha, M., Louro, R. O., Correia, I. J., Rothery, E. L., Pankhurst, K. L., Reid, G. A., Chapman, S. K., Turner, D. L., and Salgueiro, C. A. (2003) Thermodynamic characterization of a tetrahaem cytochrome isolated from a facultative aerobic bacterium, *Shewanella frigidimarina*: A putative redox model for flavocytochrome c3. *Biochem. J. 370*, 489–495.
20. Paquete, C. M., Pereira, P. M., Catarino, T., Turner, D. L., Louro, R. O., and Xavier, A. V. (2007) Functional properties of type I and type II cytochromes c3 from *Desulfovibrio africanus*. *Biochim. Biophys. Acta 1767*, 178–188.
21. Glasoe, P. K., and Long, F. A. (1960) Use of glass electrodes to measure acidities in deuterium oxide. *J. Phys. Chem. 64*, 188–190.
22. Marion, D., and Wuthrich, K. (1983) Application of phase sensitive two-dimensional correlated spectroscopy (COSY) for measurements of ^{1}H-^{1}H spin-spin coupling constants in proteins. *Biochem. Biophys. Res. Commun. 113*, 967–974.
23. Jeener, J., Meier, B. H., Bachmann, P., and Ernst, R. R. (1979) Investigation of exchange processes by two-dimensional NMR spectroscopy. *J. Chem. Phys. 71*, 4546–4553.

24. Kumar, A., Ernst, R. R., and Wuthrich, K. (1980) A two-dimensional nuclear Overhauser enhancement (2D NOE) experiment for the elucidation of complete proton-proton cross-relaxation networks in biological macromolecules. *Biochem. Biophys. Res. Commun. 95*, 1–6.
25. Brown, S. C., Weber, P. L., and Mueller, L. (1988) Toward complete (*1*)H NMR spectra in proteins. *J. Magn. Reson. 77*, 166–169.
26. Bearden, D. W., Macura, S., and Brown, L. R. (1988) Suppression of cross relaxation in TOCSY experiments on macromolecules. *J. Magn. Reson. 80*, 534–538.
27. Briand, J., and Ernst, R. R. (1991) Computer-optimized homonuclear TOCSY experiments with suppression of cross relaxation. *Chem. Phys. Lett. 185*, 276–285.
28. Griesinger, C., Otting, G., Wuethrich, K., and Ernst, R. R. (1988) Clean TOCSY for proton spin system identification in macromolecules. *J. Am. Chem. Soc. 110*, 7870–7872.
29. Rance, M., Sorensen, O. W., Bodenhausen, G., Wagner, G., Ernst, R. R., and Wuthrich, K. (1983) Improved spectral resolution in cosy ^{1}H NMR spectra of proteins via double quantum filtering. *Biochem. Biophys. Res. Commun. 117*, 479–485.
30. Derome, A. E., and Williamson, M. P. (1990) Rapid-pulsing artifacts in double-quantum-filtered COSY. *J. Magn. Reson. 88*, 177–185.
31. Bartels, C., Xia, T.-h., Billeter, M., Güntert, P., and Wüthrich, K. (1995) The program XEASY for computer-supported NMR spectral analysis of biological macromolecules. *J. Biomol. NMR 6*, 1–10.
32. Wüthrich, K. (1986) *NMR of Proteins and Nucleic Acids*, pp 30−31, 130−161, John Wiley and Sons, New York.
33. Guntert, P., Braun, W., and Wuthrich, K. (1991) Efficient computation of three-dimensional protein structures in solution from nuclear magnetic resonance data using the program DIANA and the supporting programs CALIBA, HABAS and GLOMSA. *J. Mol. Biol. 217*, 517–530.
34. Goddard, T. D., and Kneller, D. G. (2005) SPARKY, University of California, San Francisco.
35. Messias, A. C., Kastrau, D. H., Costa, H. S., LeGall, J., Turner, D. L., Santos, H., and Xavier, A. V. (1998) Solution structure of *Desulfovibrio vulgaris* (Hildenborough) ferrocytochrome c3: Structural basis for functional cooperativity. *J. Mol. Biol. 281*, 719–739.
36. Turner, D. L., Brennan, L., Meyer, H. E., Lohaus, C., Siethoff, C., Costa, H. S., Gonzalez, B., Santos, H., and Suarez, J. E. (1999) Solution structure of plantaricin C, a novel lantibiotic. *Eur. J. Biochem. 264*, 833–839.
37. Wareham, R. S., Kilburn, J. D., Rees, N. H., Turner, D. L., Leach, A. R., and Holmes, D. S. (1995) Synthesis and Solution Conformation of a C2 Symmetric Macrobicycle. *Tetrahedron Lett. 36*, 3047–3050.
38. Wareham, R. S., Kilburn, J. D., Turner, D. L., Rees, N. H., and Holmes, D. S. (1996) Homeomorphic Isomerism in a Peptidic Macrobicycle. *Angew. Chem., Int. Ed. Engl. 34*, 2660–2662.
39. Turner, D. L., Brennan, L., Chamberlin, S. G., Louro, R. O., and Xavier, A. V. (1998) Determination of solution structures of paramagnetic proteins by NMR. *Eur. Biophys. J. 27*, 367–375.
40. Guntert, P., Mumenthaler, C., and Wuthrich, K. (1997) Torsion angle dynamics for NMR structure calculation with the new program DYANA. *J. Mol. Biol. 273*, 283–298.
41. Pettersen, E. F., Goddard, T. D., Huang, C. C., Couch, G. S., Greenblatt, D. M., Meng, E. C., and and Ferrin, T. E. (2004) CSF Chimera: A Visualization System for Exploratory Research and Analysis. *J. Comput. Chem. 25*, 1605–1612.
42. Koradi, R., Billeter, M., and Wüthrich, K. (1996) MOLMOL: A program for display and analysis of macromolecular structures. *J. Mol. Graphics 14*, 51–55.
43. Vriend, G. (1990) WHAT IF: A molecular modeling and drug design program. *J. Mol. Graphics 8*, 52–56.
44. Hutchinson, E. G., and Thornton, J. M. (1996) PROMOTIF: A program to identify and analyze structural motifs in proteins. *Protein Sci. 5*, 212–220.
45. Williamson, M. P., and Asakura, T. (1993) Empirical Comparisons of Models for Chemical-Shift Calculation in Proteins. *J. Magn. Reson., Ser. B 101*, 63–71.
46. Pessanha, M., Londer, Y. Y., Long, W. C., Erickson, J., Pokkuluri, P. R., Schiffer, M., and Salgueiro, C. A. (2004) Redox characterization of *Geobacter sulfurreducens* cytochrome c7: Physiological relevance of the conserved residue F15 probed by site-specific mutagenesis. *Biochemistry 43*, 9909–9917.
47. Sarma, S., DiGate, R. J., Goodin, D. B., Miller, C. J., and Guiles, R. D. (1997) Effect of axial ligand plane reorientation on electronic and electrochemical properties observed in the A67V mutant of rat cytochrome b5. *Biochemistry 36*, 5658–5668.
48. Xue, L. L., Wang, Y. H., Xie, Y., Yao, P., Wang, W. H., Qian, W., Huang, Z. X., Wu, J., and Xia, Z. X. (1999) Effect of mutation at valine 61 on the three-dimensional structure, stability, and redox potential of cytochrome b5. *Biochemistry 38*, 11961–11972.
49. Sarma, S., Dangi, B., Yan, C., DiGate, R. J., Banville, D. L., and Guiles, R. D. (1997) Characterization of a site-directed mutant of cytochrome b5 designed to alter axial imidazole ligand plane orientation. *Biochemistry 36*, 5645–5657.

BI801326J